Journal of Power Sources 266 (2014) 36–42

Contents lists available at ScienceDirect

Journal of Power Sources

journal homepage: www.elsevier.com/locate/jpowsour

Activated nitrogen-doped carbon nanofibers with hierarchical pore as efficient oxygen reduction reaction catalyst for microbial fuel cells

Xiaoling Yang, Wenjian Zou, Yunhe Su, Yihua Zhu*, Hongliang Jiang, Jianhua Shen, Chunzhong Li

Key Laboratory for Ultrafine Materials of Ministry of Education, School of Materials Science and Engineering, East China University of Science and Technology, Shanghai 200237, China

HIGHLIGHTS

- Activated N-doped carbon nanofibers have been synthesized via a facile route.
- The stack of ANCNFs forms a 3D carbon nanofiber framework with hierarchical pores.
- The ANCNFs show better mass transfer and improved performance for ORR.
- The ANCNFs exhibit comparable MFC performance to the commercial Pt/C catalyst.

GRAPHICAL ABSTRACT

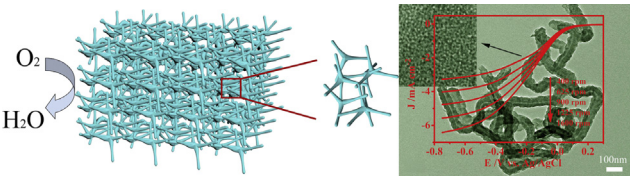

ARTICLE INFO

Article history:
Received 22 January 2014
Received in revised form
24 April 2014
Accepted 25 April 2014
Available online 10 May 2014

Keywords:
Nitrogen-doped carbon nanofibers
Hierarchically porous
Chemical activation
Oxygen reduction reaction
Microbial fuel cells

ABSTRACT

Oxygen reduction reaction (ORR) in microbial fuel cell (MFC) was evaluated by using chemical activated nitrogen-doped carbon nanofibers (ANCNFs) as cathode catalyst. ANCNFs are synthesized through modified oxidative template assembly route and then activated by KOH reagent. The as-prepared ANCNFs formed three-dimensional carbonfiber framework with large specific surface area and hierarchical tetramodal pore size distribution spanning the micro-, meso- and macro pore range, centered at 0.48, 4.0, 18 and 70 nm. Compared with unactivated nitrogen-doped carbon nanofibers (NCNFs), ANCNFs exhibited a more positive onset potential, higher current density as well as higher electron transfer number in neutral environment, highlighting the importance of chemical activation process for improving the ORR performance. MFCs equipped with ANCNFs catalyst exhibited a high power output of 1377 ± 46 mW m^{-2}, which is about 1.5 times the output of NCNFs cathode (921 ± 29 mW m^{-2}), and as high as nearly 4 times of plain cathode (341 ± 9 mW m^{-2}).

1. Introduction

Microbial fuel cells (MFCs), promising devices that convert chemical energy stored in organic matter to electricity through the catalysis of microorganisms, have attracted wide-ranging interest in recent years [1]. Many challenges, such as the technical issues associated with the performance and stability, must be overcome before MFCs are practical for renewable energy production. Among those challenges, the sluggish kinetics of oxygen reduction reaction (ORR) in the cathode and high cost of constructing MFCs is considered to be the most formidable [2]. Platinum (Pt) catalyst has long been regarded as the best catalyst for ORR at the cathode of MFCs, but Pt catalysts can even account for half of the MFCs cost. In addition, A further weakness of Pt catalyst is based on its actual strength – its versatility to serve as oxidation as well as reduction catalyst.

* Corresponding author. Tel.: +86 21 64252022; fax: +86 21 64250624.
E-mail address: yhzhu@ecust.edu.cn (Y. Zhu).

http://dx.doi.org/10.1016/j.jpowsour.2014.04.126
0378-7753/

Thus, the permeation of fuel from the anode through the polymer electrolyte membrane into the cathode compartment (fuel crossover) leads to the formation of mixed potentials and the flow of internal currents, causing a depolarization of the electrode even at open circuit [21]. Therefore, the development of Pt-free catalysts with high ORR activity, better durability and lower cost is highly desirable [3].

Currently, substantial non-noble metal based catalysts (NNMCs) have been investigated as substitute for Pt as ORR catalyst, such as hierarchical interconnected macro-/mesoporous Co-containing N-doped carbon [4], nitrogen-enriched core–shell structured Fe/Fe_3C–C nanorods (N–Fe/Fe_3C@C) [5], nanocomposite of Co_3O_4 and nitrogen-doped graphene (Co_3O_4/N–G) [6]. However, for the most metal-containing NNMCs, they frequently suffer from dissolution, sintering, and agglomeration during fuel cell operation which can reduce activity and durability [7]. Hence, the development of metal-free catalysts that exhibit superior activity toward ORR is more warranted.

Carbon-based nanomaterials, such as nanotubes and graphene, have been extensively demonstrated as a potential substitute for Pt to reduce the cost and enhance the stability. Feng et al. investigated the ORR catalytic activity of nitrogen-doped carbon nanotubes (NCNTs) and nitrogen-doped graphene (NG), indicating that NCNTs and NG showed comparable electrocatalytic activity and power performances to Pt/C, and better durability for cathodic ORR than Pt/C [8]. Furthermore, the NCNTs and NG were applied as cathode catalysts for the ORR process in MFCs and obtained power performances comparable to those of conventional platinum catalysts [9]. Ghasemi et al. reported applying activated carbon nanofibers (ACNFs), which used PAN as precursor, as an alternative cathode catalyst to platinum in a two-chamber MFC, and produced a power density of 61.3 mW m^{-2} [10].

Though reveal a promising substitute for Pt, there is still huge potential to boost the catalytic activity of metal-free catalyst. Comprehensive studies suggested possible requirements for obtaining high active catalyst, including high electrical conductivity, large surface area and hierarchical pore structure. However, most reported metal-free catalysts cannot satisfy all the features mentioned above simultaneously. Thus, designing a hierarchical porous nitrogen-doped carbon based materials can possibly meet the requirement of ORR catalyst.

Morozan et al. investigated the relationship between the morphology of polypyrrole and their electrocatalytic performances towards ORR in alkaline media and confirmed that annealed polypyrrole with granular- and tubules-like morphology exhibited different catalytic efficiencies [11], which shed light to the affection of different morphology to ORR catalytic activity. Thus, in this study, we prepared a nitrogen-doped carbon nanofibers (NCNFs) with clip-like morphology with polypyrrole as reported previously [12], and the activated NCNFs (ANCNFs) through a chemical activation process of KOH, which are low cost and easily accessible. The electrocatalytic activities of synthesized NCNFs and ANCNFs for ORR in the neutral pH medium were also examined for investigating the effect of chemical activation process. Moreover, we applied NCNFs and ANCNFs as cathode catalysts in MFCs to evaluate the feasibility of NCNFs and ANCNFs in biological systems, and their performance were compared with the commonly used Pt catalyst.

2. Experimental

2.1. Materials

All the chemicals were of analytical grade and used without any further purification, and purchased from Shanghai Chemical Reagent Co. Ultrapure water (18 MΩ cm) was used for all experiments.

2.2. Preparation of NCNFs and ANCNFs

The clip-like polypyrrole precursor was synthesized via a modified oxidative template assembly route [13]. Typically, cetrimonium bromide (CTAB, $(C_{16}H_{33})N(CH_3)_3Br$, 7.3 g) was first dissolved in HCl solution (120 mL, 1 mol L^{-1}) under ice bath. After stirred for 10 min, pyrrole monomer (8.3 mL) was added into the solution. The reaction was carried out at 0 °C for 24 h. After that, the resulted product was collected by centrifugation and washed with 1 mol L^{-1} HCl solution and water until the filtrate became colorless and neutral. Finally, the obtained black product was dried overnight at 70 °C in an oven.

The NCNFs were prepared by heating the as-obtained clip-like polypyrrole to the set temperature with a heating rate of 5 °C per minute and keeping for 2 h under argon atmosphere. ANCNFs were synthesized through chemical activation of the clip-like polypyrrole. Typically, 0.25 g sythesized polypyrrole was dispersed in 10 mL H_2O, and 0.25 g KOH was dissolved in the suspension. The solvent was then evaporated in 80 °C. After that, the mixture of KOH and polypyrrole was moved to a nickel crucible and then heated to 900 °C with a heating rate of 5 °C per minute and kept for 2 h under argon atmosphere. The pyrolyzed product was then collected by centrifugation and washed with 1 mol L^{-1} HCl solution and water until the filtrate became neutral. Finally, the obtained black product was dried overnight at 70 °C in an oven.

2.3. Material and electrochemical analyses

The catalyst ink formulation used in electrochemical measurements and MFC tests was the same: 1 mg of catalyst was dispersed in 1 mL of a solvent mixture of Nafion (5 wt %) and anhydrous ethanol (1:9, v:v) for 0.5 h under sonication.

For the electrochemical tests, a 10 μL portion of catalyst suspension was lightly deposited dropwise onto a prepolished glass carbon electrode diameter of 3 mm (catalyst loading: 0.14 mg cm^{-2}). Commercial 20% Pt/C catalyst electrode was prepared in the same procedure mentioned above.

For MFC cathode fabrication, the catalysts ink was brushed onto a 2 cm by 2 cm carbon paper, and the catalysts loading on the carbon paper was 1 mg cm^{-2}.

To demonstrate the overall morphology and structure, the samples were examined by scanning electron microscopy (SEM), using a JEOL Model SM-6360LV microscope (JEOL, Japan), and transmission electron microscopy (TEM), with a JEOL Model 2011 microscope (JEOL, Japan) operated at 200 kV. The crystalline structure was investigated by powder X-ray diffraction (XRD) (Rigaku, Model D/MAX 2550 VB/PC, Japan).

Electrochemical measurements of linear sweep voltammetry (LSV) and chronoamperometric response (i–t curve) were carried out with a Model CHI 660C electrochemical workstation (CH Instruments, Chenhua Instrument Co., China) connected to a personal computer. A three-electrode configuration was employed, consisting of glassy carbon electrode (3 mm in diameter) or glassy carbon rotating disk electrode (5 mm in diameter) serving as the working electrode, Ag/AgCl (3 M KCl) reference electrode and platinum wire counter electrode, respectively. The working electrode coated with catalyst ink is allowed to dry at room temperature (25 °C) before measurement. 100 mM PBS saturated with oxygen served as the supporting electrolyte. The linear sweep voltammograms (LSVs) were recorded in O_2 saturated 100 mM PBS between −0.75 and 0.4 V with a scan rate of 10 mV s^{-1} at various rotating speeds from 400 to 1600 rpm. After each scan, the electrolyte was saturated with O_2 again for 5 min. Koutecky–Levich plots were analyzed at different electrode potentials. The electron transfer number (n) of

the resulting HP–Fe–N–C was analyzed on the basis of the K–L equations.

The power density ($P = IV/A$) for the MFCs was measured by a Model 2400 Source Meter (Keithley, Cleveland, OH), according to the measured voltage (V), current ($I = V/R$), and surface area of the cathode electrode (A). The maximum power output was determined by the polarization curves.

2.4. MFC construction and operation

In this study, the MFC experiments were carried out in a self-made two-chamber H-type MFC which we reported previously [4]. The anode chamber was filled with mixed cultures, carbon granules (diameters of 1–3 mm) and sodium acetate (1000 mg L^{-1}) culture medium solution. The culture medium solution contained: phosphate buffer solution (PBS, 100 mM) and mineral solution (12.5/1000 v/v). The catholyte in cathode chamber was 100 mM PBS. Air was purged into the cathode compartment in order to supply the oxygen needed for the electrochemical reaction.

The MFCs were inoculated with the wastewater from the sewage treatment plant of the East China University of Science and Technology (Shanghai, China). After replacement of this culture medium solution three times over 7 days, the system was then operated using only the nutrient medium and sodium acetate. The system was considered to be operating under steady conditions when the maximum voltage output was reproducible after refilling the reactor with medium at least two times. The medium in the reactor was refilled when the voltage dropped below 30 mV.

All tests were conducted at room temperature. The power and current density were normalized by the projected surface area of the cathode (4 cm^{-2}). All tests were conducted in duplicate, and mean values are presented.

The number of the independent biological replicates (n) for all materials (ANCNFs, NCNFs, Pt/C and plant cathode) was 5.

3. Results and discussion

The polypyrrole precursor was synthesized via a modified oxidative template assembly method [13]. As shown in Fig. 1a, the SEM image of polypyrrole shows the clip-like morphology with a diameter of 160 nm. While for NCNFs (Fig. 1b) and ANCNFs (Fig. 1c), their morphology are akin to the polypyrrole precursor but with a decreased diameter from 160 to 70 nm and some curving carbon nanofibers are observed, which can be attributed to the pyrolysis treatment. The transmission electron microscopy (TEM) image of ANCNFs further demonstrated the clip-like nanofiber morphology (Fig. 1d), and a tunnel can be clearly observed in the middle of nanofibers, which is consistent with the previous reports [12]. Both NCNFs and ANCNFs elucidated the same cross-linked microstructure. However, the high-resolution transmission electron microscopy (HRTEM) image (the inset of Fig. 1d) reveals that large quantities of micropores are homogeneously distributed within ANCNFs, which may be generated due to the chemical activation of KOH.

The structure of ANCNFs and NCNFs were then studied by XRD measurement. As shown in Fig. 2, no other diffraction peaks are observed in the XRD patterns except for the C (002) diffraction peak, indicating the amorphous state of ANCNFs and NCNFs. Nevertheless, the sharper diffraction peak and higher intensity of ANCNFs may reveal a higher graphitization degree than NCNFs.

To further study the pore structure of ANCNFs and NCNFs, N_2 adsorption–desorption isothermal analysis was performed. The BET surface area of ANCNFs and NCNFs are 1983.5 and 30.9 $m^2\ g^{-1}$, with a total pore volume of 1.41 and 0.11 $cm^3\ g^{-1}$, respectively (BJH model). As shown in Fig. 3a, the NCNFs exhibit a combination of II/III type adsorption–desorption isothermal with H_3 hysteresis loops but with no N_2 adsorption at low pressure, revealed weak interaction between NCNFs and nitrogen. While the ANCNFs (Fig. 3b) show a combination of I/IV type adsorption–desorption isothermal with N_2 adsorption at low pressure and steep adsorption at the high relative pressure (0.9–1.0 P/P_o), which confirmed strong interaction between ANCNFs and nitrogen and indicate the coexistence of mesopores and micro-pores. From the pore size distribution (PSD) plot (insets in Fig. 3), it can be seen that NCNFs possess continuous pores distribution in the range 20–60 nm and small mesopores peaked at 3.85 nm and 4.87 nm. The ANCNFs mainly possess micropores and small meso-pores peaked at 4 nm as well as large mesopores (peaked at 8 nm) and macropores. For ANCNFs, micropores area is only 269.1 $m^2\ g^{-1}$, taking 13.6% of the whole BET surface area, which revealed the large numbers of mesopores.

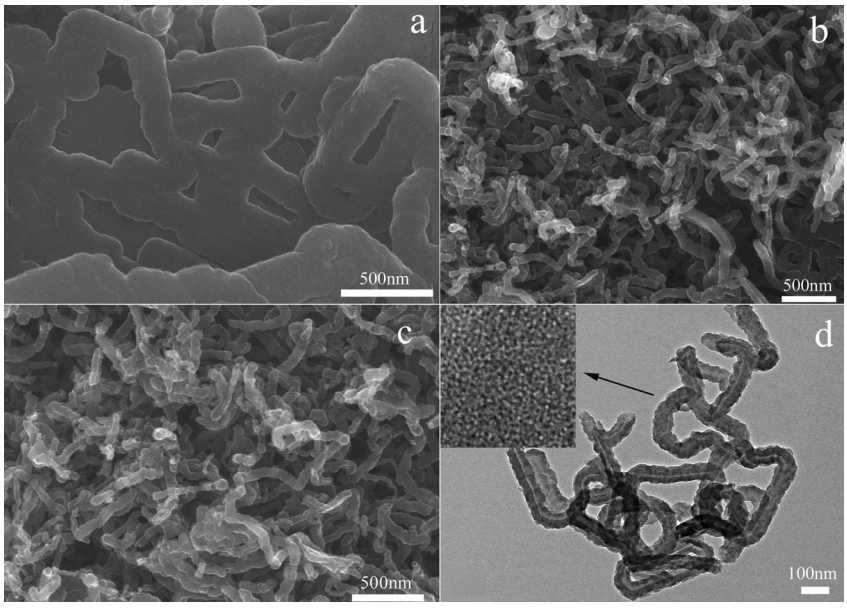

Fig. 1. SEM images of PPy nanofiber (a), NCNFs (b), ANCNFs (c) and TEM image of ANCNFs (d). The inset is the HRTEM image of ANCNFs.

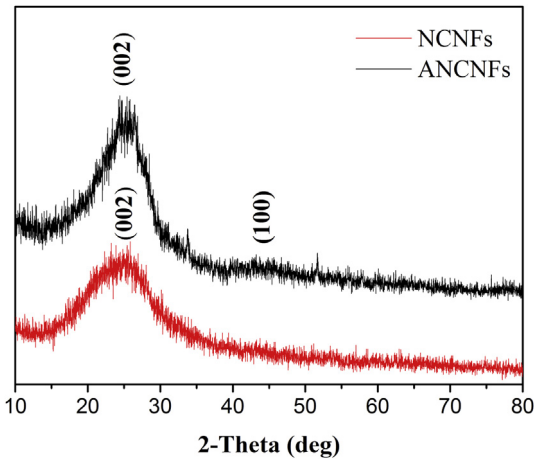

Fig. 2. XRD pattern of NCNFs (a) and ANCNFs (b).

It is particularly worth mentioning that stack of nanofibers produced a three-dimensional carbon nanofiber framework and resulted in the formation of large meso-pores and macro-pores mentioned above, which can be proved by the PSD plot and appearance of H_3 hysteresis loops of NCNFs. Because of the similar morphology of ANCNFs and NCNFs, such three-dimensional structure also exists in ANCNFs. But because of the low pore volume of macro-pores and large meso-pores and interference of other types of hysteresis loops, it cannot be clearly observed in the N_2 adsorption–desorption isothermal and PSD image of ANCNFs. The micro-meso- and macro-pores coexistence three-dimensional structure and large specific surface area can contribute to accessible part of active site and transport properties of ORR relevant species (O_2, H^+, H_2O, e^-). The more exposure of active sites and enhanced transfer efficiency can surely lead to higher catalytic.

To probe the chemical identities of the heteroatoms in the NCNFs and ANCNFs, X-ray photoelectron spectroscopic (XPS) measurement was carried out. It is believed that carbon atoms adjacent to nitrogen dopants possess a substantially high positive charge density to counterbalance the strong electronic affinity of the nitrogen atom. The nitrogen-induced charge delocalization could also alter the adsorption behavior of carbon-based material toward oxygen, which effectively weakening the O–O bonding to facilitate the ORR process [14]. From this point, nitrogen doping may affect ORR activity to a large extent. Peaks of C1s, N1s and O1s were observed in survey spectra of NCNFs and ANCNFs (Fig. 4a), both of the two samples show relatively high nitrogen content (19.1% and 10.1% respectively).

The high resolution C1s spectrum of NCNFs (Fig. 4c) and ANCNFs (Fig. 4e) can be deconvoluted into four individual peaks, corresponding to C–C (284.6 eV), C–N (285.3 eV), C–O (286.5 eV) and CO (288.2 eV), proved the successfully the doping of nitrogen into the carbon frameworks. High resolution N1s spectrums of both NCNFs and ANCNFs were collected to gain more insight into nitrogen doping. As shown in Fig. 4d and f, the high resolution N1s spectrum can be fitted into three chemical states peaks, which are corresponding to pyridinic-N (398.4 eV), pyrrolic-N (399.9 eV) and graphitic-N (400.8 eV), respectively. Content of each nitrogen component is shown in Table 1. During the high temperature pyrolysis, pyrrole-N may partly converted to pyridinic- and graphitic-N, leading to an increase in graphitic- and pyridinic-N and a decrease in pyrrole-N. Compared with NCNFs, ANCNFs reveal higher graphitic-N and lower pyrrole-N content, suggesting the higher graphitization degree, which is consistent with the XRD result. The graphitic-N is a type of nitrogen that bonds to three carbon atoms in the carbon plane. It is reported that the graphitic-N could serve as ORR catalytic sites both experimentally and theoretically due to the reduced adsorption energy, and also can greatly increase the limiting current density [15–18]. In addition, there is no lone pair of electrons around graphitic-N in the carbon plane, so it is less susceptible to protonation reaction and may contribute to stability of the catalyst. From what has been discussed above, it could be inferred that the ANCNFs may possess better ORR activity than the NCNFs.

Linear-sweep voltammograms (LSVs) tests were first carried out in O_2-saturated 100 mM PBS medium by using a rotating disk electrode (RDE) to investigate the electrocatalytic activity and kinetics of the NCNFs and ANCNFs catalysts. The ORR onset potential of each sample was acquired from RDE linear swap at 1600 rpm. LSVs for NCNFs samples with different pyrolysis temperature ranging from 800 to 1000 °C were shown in Fig. S1 (denoted as NCNF-800, NCNF-900 and NCNF-1000, respectively). The NCNFs-900 showed not only the largest limiting current density but also the most positive onset potential (−0.05 V, vs Ag/AgCl). Similar phenomenon can also be observed in ANCNFs samples (Fig. S1b), samples pyrolysis in 900 °C revealed better onset potential and limiting current density. Therefore, 900 °C could be the optimal pyrolysis temperature.

LSVs for NCNFs-900, ANCNFs pyrolysis in 900 °C (denoted as ANCNFs-900) and commercial Pt/C at 1600 rpm were shown in Fig. 5a. The limiting current density and onset potential are two important criterion to evaluate the ORR activity of catalysts.

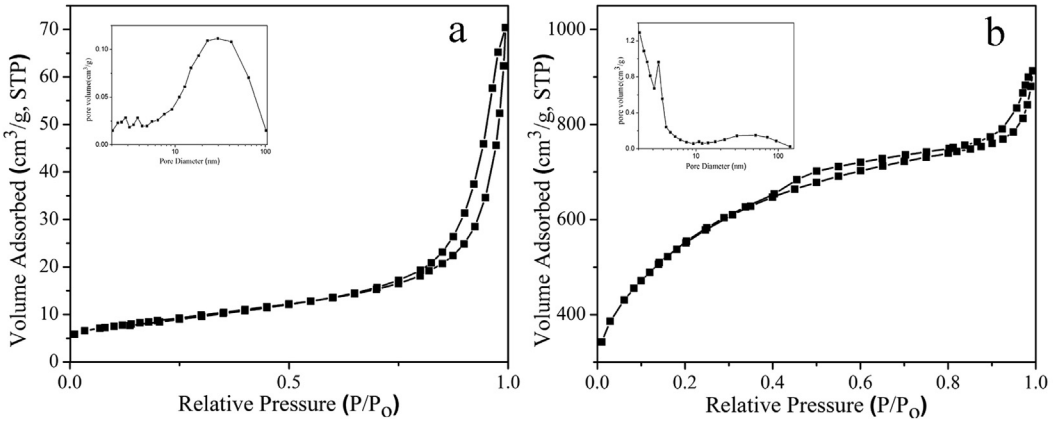

Fig. 3. N_2 adsorption–desorption isotherms of NCNFs (a) and ANCNFs (b). Inset are the corresponding pore size distributions (PSD).

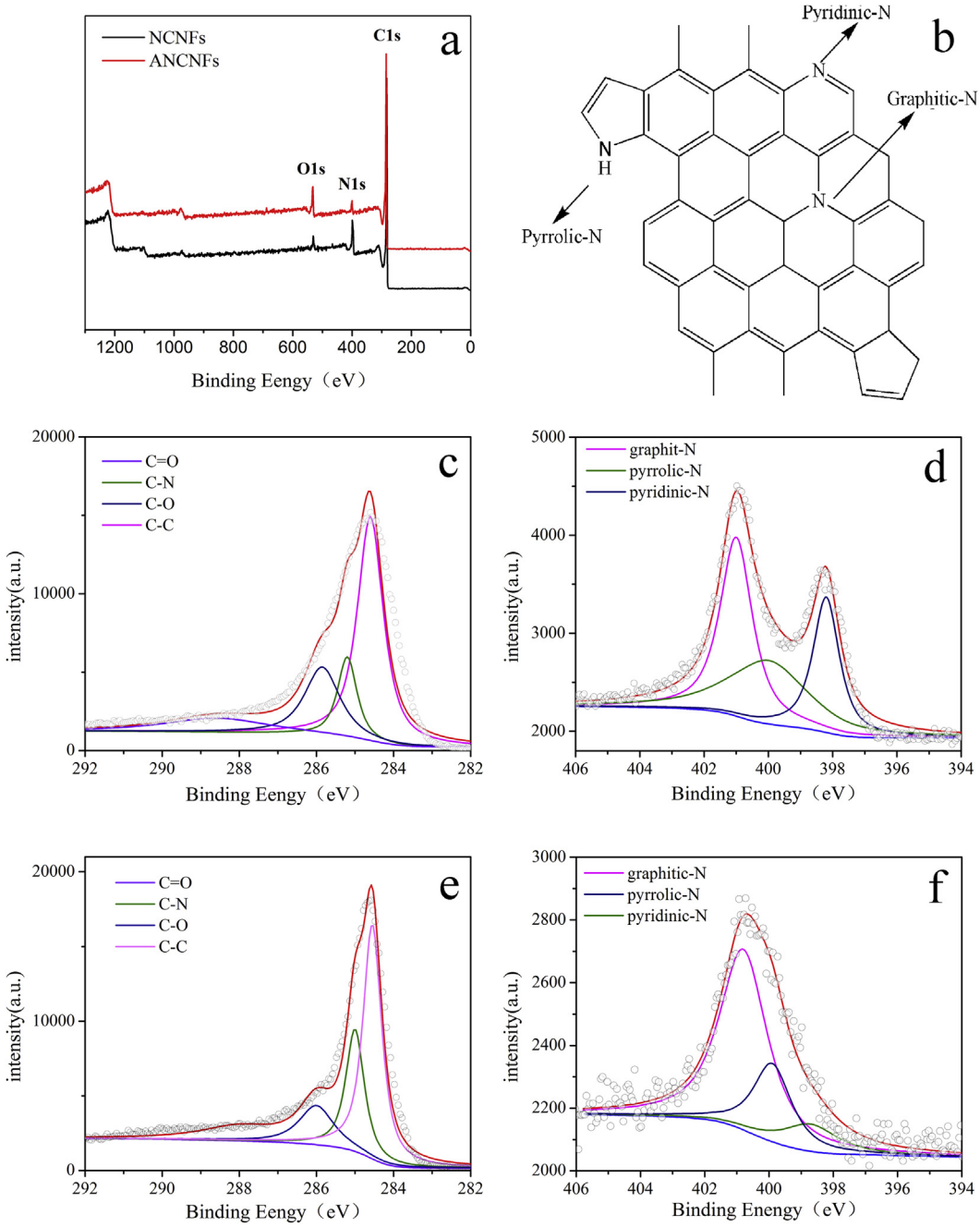

Fig. 4. XPS survey spectra of NCNFs and ANCNFs (a), schematic representation of NCNFs and ANCNFs (b), core level XPS spectra C1s (c), N1s (d) of NCNFs, and C1s (e), N1s (f) of ANCNFs.

Apparently, in both limiting current density and onset potential, NCNFs are significantly inferior to ANCNFs. Onset potential of ANCNFs have greatly increased positively compared with NCNFs (0.12 V vs −0.05 V), and limiting current density increased to almost twice of the NCNFs. Compared with commercial Pt/C catalyst, though exhibited negative onset potential, ANCNFs exhibited larger limiting current density when potential shifted negatively from −0.50 V.

Table 1
Content of each nitrogen component.

	Graphitic-N	Pyrrolic-N	Pyridinic-N
NCNFs	40.59%	34.34%	25.07%
ANCNFs	65.83%	22.62%	11.54%

For further insight into the ORR kinetics of the NCNFs and ANCNFs, Koutecky–Levich (K–L) plots were obtained from the LSV curve (Fig. S1a and Fig. 5c). The K–L plots were obtained by linear fitting of the inverse square root of rotating speed vs reciprocal current density at rotation rate from 400 to 1600 rpm. LSVs for ANCNFs (Fig. 5b) showed the increasing current density with increased rotation rate, which can be explained by shorten diffusion distance at high speed and agrees with the previous report [19]. The electron transfer numbers involved in a typical ORR process can be calculated from the slopes of K–L equation as follows:

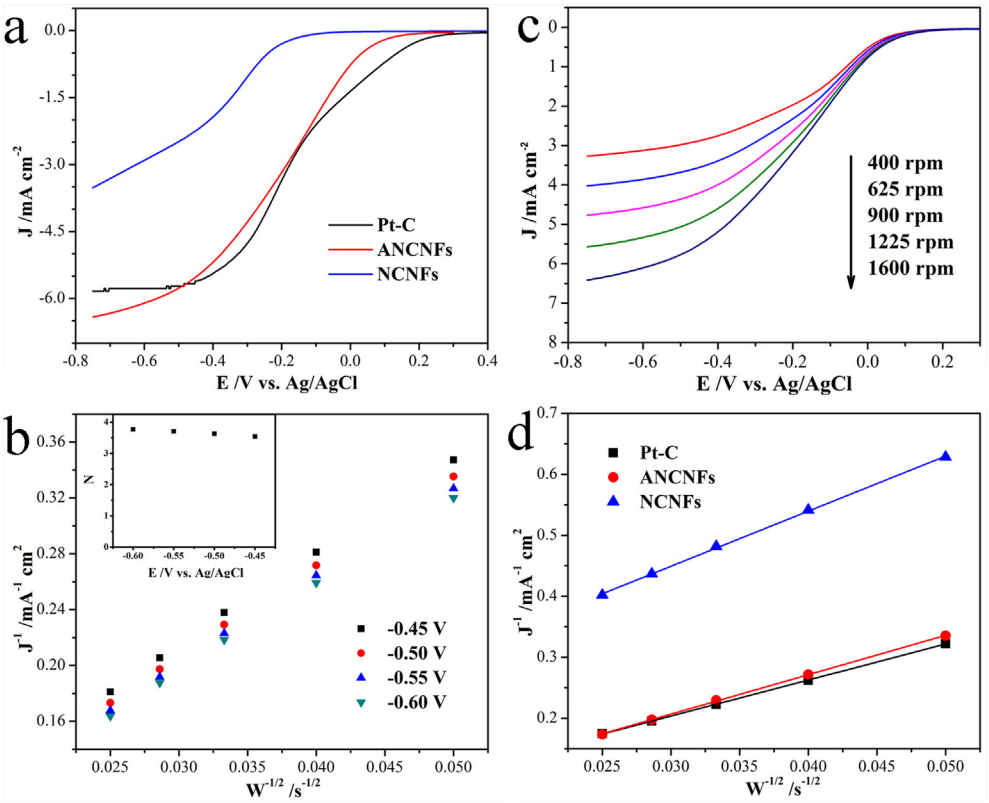

Fig. 5. LSVs for different samples in O_2-saturated neutral PBS at a rotating speed of 1600 rpm (a), LSVs for ANCNFs at different rotation rates (b), K–L plots and the corresponding electron transfer numbers of ANCNFs (c), K–L plots for different samples at −0.50 V (d).

$$\frac{1}{J} = \frac{1}{J_L} + \frac{1}{J_K} = \frac{1}{B\omega^{1/2}} + \frac{1}{J_K} \quad (1)$$

$$B = 0.62nFC_0(D_0)^{2/3}\nu^{-1/6} \quad (2)$$

where n is the number of electrons transferred per oxygen molecule, F is the Faraday constant (96,485 C mol^{-1}), C_0 is the concentration of O_2 (1.2×10^{-3} mol L^{-1}), D_0 is the diffusion coefficient of O_2 in 0.1 M PBS and ν is the kinetic viscosity, The constant 0.62 is adopted when the rotating speed is in rad s^{-1}.

The K–L plots of all materials prepared reveal good linear (Fig. 5d) and the electrons transferred number of the NCNFs and ANCNFs were 2.5 and 3.6 (−0.5 V, inset Fig. S2, inset Fig. 5c), respectively, indicating a nearly two-electron pathway for NCNFs and a nearly four-electron pathway for ANCNFs. The polarization curve of Pt/C and corresponding K–L plots was also obtained under the same experimental condition (Fig. S2d). The electrons transferred number of Pt/C in our study was calculated to be 4.0 in neutral condition (inset Fig. S2d).

In association with the XPS measurement and N_2 adsorption–desorption isothermal analysis result discussed above, the good catalytic activity probably largely depend on the content of graphitic-N and three-dimensional hierarchical pore structure. The overall ORR rate is determined by the surface reaction rate on the catalyst in the low overpotential region, while the overall ORR rate is dependent on the oxygen diffusion in the high overpotential region [20]. In this regard, the three-dimensional hierarchical pore structure combined the positive effect of macro-pores on diffusion and sufficient amount of active sites, which linked to high specific surface area, thus promote ORR activities. These may shed light on the excellent ORR catalytic activity of ANCNFs.

The long-term stability is of catalyst is another major concerns in MFCs technology. The ANCNFs shows higher stability than that of Pt/C with only a small attenuation (85.1% compared to 64.0% of Pt/C) during a 5.56 h testing period in O_2 0.1 M PBS (Fig. 6). ANCNFs possess higher content of graphitic nitrogen atoms and the graphitic-N is a type of nitrogen that bonds to three carbon atoms in the carbon plane. There is no lone pair of electrons around graphitic-N in the carbon plane, so it is less susceptible to protonation reaction which may explains the high stability.

The aqueous cathode H-shaped MFCs equipped with NCNFs, ANCNFs, Pt/C cathode catalysts and without cathode catalyst were set up for further study ORR performances of the catalysts prepared. Fig. 7 shows the polarization curves and power density curves of MFCs with NCNFs, ANCNFs, Pt/C as cathode catalysts and

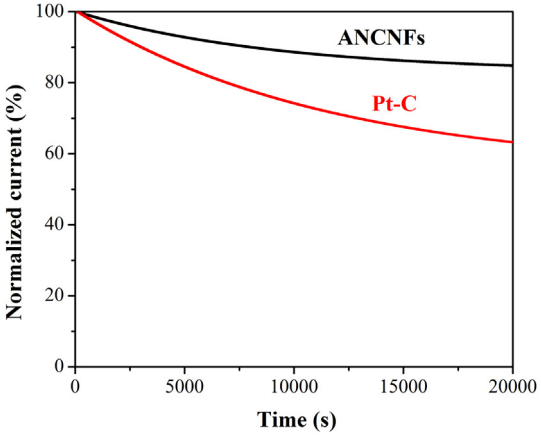

Fig. 6. Chronoamperometric response of ANCNFs and Pt/C in O_2-saturated 0.1 M PBS.

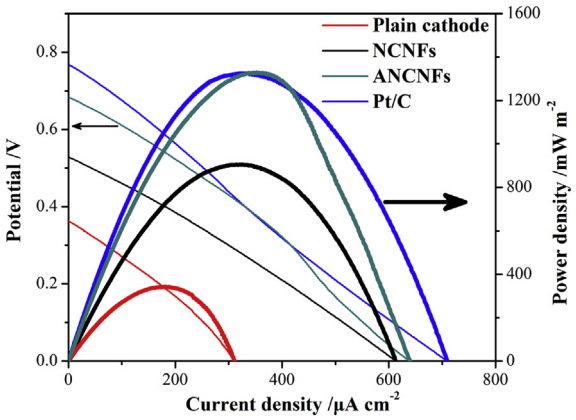

Fig. 7. Polarization curves and power density curves of MFCs with cathode catalysts of NCNFs, ANCNFs and Pt/C and without catalyst.

with the plain cathode (denoted as NCNFs-MFC, ANCNFs-MFC, Pt/C-MFC and Plain-MFC, respectively).

The open-circuit voltages of NCNFs-MFC, ANCNFs-MFC, Pt/C-MFC and Plain-MFC were 0.54 V, 0.74 V, 0.71 V and 0.19 V, respectively. Based on the polarization data, the maximum power density in ANCNFs-MFC was 1377 ± 46 mW m^{-2}, which is as high as nearly 4 times of Plain-MFC (341 ± 9 mW m^{-2}), and only slightly higher than the Pt/C-MFC (1307 ± 43 mW m^{-2}). The NCNFs-MFC displayed a maximum power density of 921 ± 29 mW m^{-2}, which is as low as 2/3 of ANCNFs-MFC.

4. Conclusions

In summary, the activated nitrogen-doped carbon nanofibers were synthesized via a simple KOH chemical activation process and applied as metal-free cathodic catalyst in aqueous cathode of H-shaped MFC. The ANCNFs exhibited superior electrocatalytic activity than NCNFs toward ORR under neutral condition as well as near comparable ORR property to commercial Pt/C catalyst, suggesting ANCNFs a potential substitution to Pt/C catalyst. In addition, the study demonstrated that the hierarchical porous structure and chemical identities of nitrogen doping may play an important role in enhancing the ORR electrocatalytic performance of carbon materials.

Acknowledgments

This work was supported by the National Natural Science Foundation of China (21236003, 21206042, 20925621, and 21176083), the Basic Research Program of Shanghai (13NM1400700, 13NM1400701), and the Fundamental Research Funds for the Central Universities (WD1013015, WD1114005 and WD1313002).

Appendix A. Supplementary data

Supplementary data related to this article can be found at http://dx.doi.org/10.1016/j.jpowsour.2014.04.126.

References

[1] M. Zhou, M. Chi, J. Luo, H. He, T. Jin, J. Power Sources 196 (2011) 4427–4435.
[2] S.J. Guo, S. Zhang, S.H. Sun, Angew. Chem. Int. Ed. 52 (2013) 8526–8544.
[3] B. Wang, J. Power Sources 152 (2005) 1–15.
[4] H. Jiang, Y. Su, Y. Zhu, J. Shen, X. Yang, Q. Feng, C. Li, J. Mater. Chem. A 1 (2013) 12074–12081.
[5] Z. Wen, S. Ci, F. Zhang, X. Feng, S. Cui, S. Mao, S. Luo, Z. He, J. Chen, Adv. Mater. 24 (2012) 1399–1404.
[6] Y. Su, Y. Zhu, X. Yang, J. Shen, J. Lu, X. Zhang, J. Chen, C. Li, Ind. Eng. Chem. Res. 52 (2013) 6076–6082.
[7] D.S. Yang, D. Bhattacharjya, S. Inamdar, J. Park, J.S. Yu, J. Am. Chem. Soc. 134 (2012) 16127–16130.
[8] L.Y. Feng, Y.G. Chen, L. Chen, ACS Nano 5 (2011) 9611–9618.
[9] L. Feng, Y. Yan, Y. Chen, L. Wang, Energy Environ. Sci. 4 (2011) 1892–1899.
[10] M. Ghasemi, S. Shahgaldi, M. Ismail, B.H. Kim, Z. Yaakob, W.R.W. Daud, Int. J. Hydrogen Energy 36 (2011) 13746–13752.
[11] A. Morozan, P. Jégou, S. Campidelli, S. Palacin, B. Jousselme, Chem. Commun. 48 (2012) 4627–4629.
[12] L. Qie, W.M. Chen, Z.H. Wang, Q.-G. Shao, X. Li, L.X. Yuan, X.L. Hu, W.X. Zhang, Y.H. Huang, Adv. Mater. 24 (2012) 2047–2050.
[13] L. Zhen, X.Y. Zhang, S. Poyraz, S.P. Surwade, S.K. Manohar, J. Am. Chem. Soc. 132 (2010) 13158–13159.
[14] K. Gong, F. Du, Z. Xia, M. Durstock, L. Dai, Science 323 (2009) 760–764.
[15] H. Kim, K. Lee, S.I. Woo, Y. Jung, Phys. Chem. Chem. Phys. 13 (2011) 17505–17510.
[16] L.F. Lai, J.R. Potts, D. Zhan, L. Wang, C.K. Poh, C.H. Tang, H. Gong, Z.X. Shen, J.Y. Lin, R.S. Ruoff, Energy Environ. Sci. 5 (2012) 7936–7942.
[17] E.J. Biddinger, U.S. Ozkan, J. Phys. Chem. C 114 (2010) 15306–15314.
[18] R.L. Liu, D.Q. Wu, X.L. Feng, K. Mullen, Angew. Chem. Int. Ed. 49 (2010) 2565–2569.
[19] R. Bashyam, P. Zelenay, Nature 443 (2006) 63–66.
[20] J. Liang, Y. Zheng, J. Chen, J. Liu, D.H. Jurcakova, M. Jaroniec, S.Z. Qiao, Angew. Chem. Int. Ed. 51 (2012) 1–6.
[21] F. Harnisch, S. Wirth, U. Schröder, Electrochem. Commun. 11 (2009) 2253–2256.